ROBUST OP AMP REALIZATION OF CHUA'S CIRCUIT

by

Michael Peter Kennedy

Memorandum No. UCB/ERL M92/26

5 January 1992

ROBUST OP AMP REALIZATION OF CHUA'S CIRCUIT*

Michael Peter Kennedy
Electronics Research Laboratory
University of California, Berkeley, CA 94720

Abstract

Chua's circuit is a simple electronic network which exhibits a variety of bifurcation phenomena and attractors. The circuit consists of two capacitors, an inductor, a linear resistor, and a nonlinear resistor (henceforth called the Chua diode). This paper describes the design methodology for a robust practical op amp implementation of Chua's circuit. In addition, we present experimental results and SPICE simulations for a working circuit using off-the-shelf components.

1 Introduction

Chua's circuit [Mat84], shown in Fig. 1, is a simple oscillator circuit which exhibits a variety of bifurcations and chaos. The circuit contains three linear energy-storage elements (an inductor and two capacitors), a linear resistor, and a single nonlinear resistor N_R. The state equations for the circuit are as follows:

$$
\begin{aligned}
C_1 \frac{dv_{C_1}}{dt} &= G(v_{C_2} - v_{C_1}) - g(v_{C_1}) \\
C_2 \frac{dv_{C_2}}{dt} &= G(v_{C_1} - v_{C_2}) + i_L \\
L \frac{di_L}{dt} &= -v_{C_2}
\end{aligned}
\tag{1}
$$

where $G = 1/R$ and $g(\cdot)$ is a *piecewise-linear* function defined by:

$$
g(v_R) = m_0 v_R + \frac{1}{2}(m_1 - m_0) \left[|v_R + B_p| - |v_R - B_p| \right]
\tag{2}
$$

This relation is shown graphically in Fig. 2; the slopes in the inner and outer regions are m_0 and m_1 respectively; $\pm B_P$ denote the breakpoints. The nonlinear resistor N_R is termed *voltage-controlled* because the current in the element is a function of the *voltage* across its terminals.

In the first reported study of this circuit, Matsumoto [Mat84] showed by computer simulation that the system possesses a strange attractor called the Double Scroll. Experimental confirmation of the presence of this attractor was made shortly afterwards by Zhong and Ayrom [ZA85a]. Since then, the system has been studied extensively; a variety of bifurcation phenomena and chaotic attractors in the circuit have been discovered experimentally and confirmed mathematically [CKM86, KC87, MC87, Kah88a, Kah88b, Kah88c, Kom88a, Kom88b, MCA88, Kom90, Kah91, KTMH91, LU91].

Most of the experimental studies of Chua's circuit have appeared in the circuit theory literature [MCK85, MCK86, Bro87, MCK87, Ogo87, YL87, BT90]. This work is directed at a broader audience of electronics engineers who are excited by nonlinear dynamics but who have little or no training in nonlinear circuits. Our aim is to provide the necessary circuit theoretical background and practical details to assist the experimentalist in studying Chua's circuit.
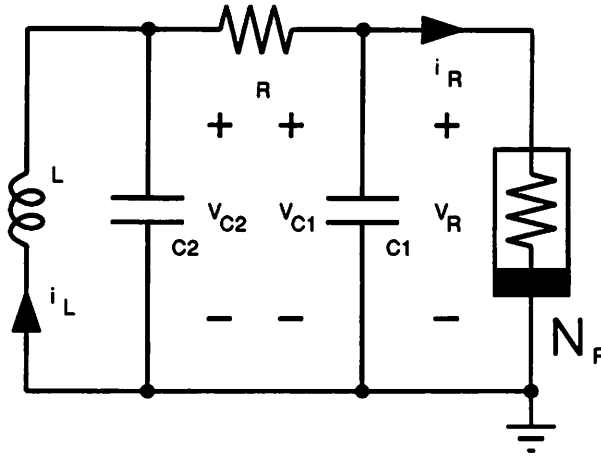

Figure 1: Chua's circuit consists of a linear inductor L, a linear resistor R, two linear capacitors C_1 and C_2, and a nonlinear resistor N_R.
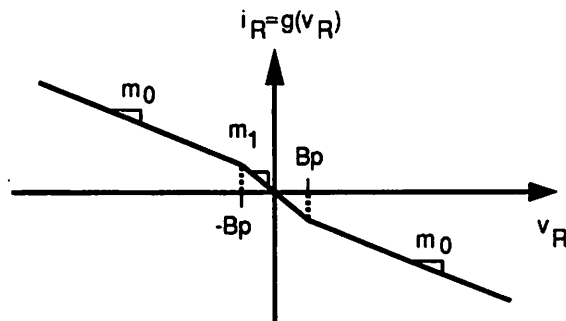

Figure 2: Three-segment piecewise-linear $v - i$ characteristic of the nonlinear resistor in Chua's circuit. The outer regions have slopes m_0; the inner region has slope m_1. There are two breakpoints at $\pm B_P$.

While differential equations and mechanical systems provide convenient frameworks in which to examine bifurcations and chaos, electronic circuits are unique in being easy to build, easy to measure, and easy to model. Furthermore, they operate in real time, and parameter values are readily adjusted. The importance of Chua's circuit and its relatives [MCT87, PC87a, Wu87, BC88, SC88, CL90a] is that they can exhibit *every* type of bifurcation and attractor which has been reported to date in third-order continuous-time dynamical systems [ZA85b, TMIM89, TMK+89, CL90b]. While exhibiting a rich variety of complex dynamical behaviors, the circuits are simple enough to be constructed and modeled using standard electronic parts and simulators.

In this work, we show how to build Chua's circuit using off-the-shelf components. We describe in detail the design methodology which has been followed for constructing the appropriate nonlinear resistor (henceforth called the *Chua diode*), and present experimental and simulation results for an example circuit.

2 Practical realization of Chua's circuit

Chua's circuit can be realized in a variety of ways using standard or custom-made electronic components. Since all of the linear elements (capacitor, resistor, and inductor) are readily available as two-terminal devices, our principal concern here will be with circuitry to realize the Chua diode.

Several implementations of this element already exist in the literature; these use diodes [Mat84], operational amplifiers [ZA85a], transistors [MCT86], and operational transconductance amplifiers [CC91].

The circuit which we present in the following sections is for demonstration, research, and educational purposes. While it may appear more complicated than earlier implementations in that the nonlinear resistor comprises two operational amplifiers (op amps), it is possible to buy two op amps in a single package. Thus, our circuit uses a minimum number of components: a pair of op amps and six resistors to implement the Chua diode, two capacitors, an inductor, and a variable resistor.

From computer simulation to experiment: scaling of current and time

Matsumoto et al. [MCK85] have shown by computer simulation of equation (1) that a Double Scroll attractor appears in Chua's circuit for the following values of the parameters:

$$C_1 = 1/9; C_2 = 1; L = 1/7; G = 0.7; B_P = 1; m_0 = -0.5; m_1 = -0.8.$$

In these and his earlier simulations, no units were given (or needed) for the state variables v_{C_1}, v_{C_2}, and i_L since Matsumoto was simply simulating a set of differential equations. If we rewrite the equations in SI units, then the voltages are measured in Volts (V), currents in Amperes (A), capacitance in Farads (F), inductance in Henrys (H), and resistance in Ohms (Ω); the reciprocal of resistance, called conductance, is measured in Siemens (S).

Since currents of milliAmperes are easier to realize in electronic circuits than Amperes, the first step is to rescale all currents by a factor of 1000; the effect is to reduce all capacitances by a factor of 1000 and to increase resistances and inductances by the same factor. Thus, with v_{C_1} and v_{C_2} in units of Volts and i_L in milliAmperes, Matsumoto's set of parameters becomes:

$$
\begin{aligned}
C_1 &= 1/9 \times 10^{-3}\text{F} \\
C_2 &= 1 \times 10^{-3}\text{F} \\
L &= 1/7 \times 10^{3}\text{H} \\
G &= 0.7 \times 10^{-3}\text{S}
\end{aligned}
$$

The slopes of the piecewise-linear resistor are now -0.8 mS (mA/V) and -0.5 mS; the breakpoints remain unchanged at $B_P = 1$ V.

It is easier to use capacitances of nF and inductances of mH than Farads and Henrys, respectively. The effect of rescaling time in equation (1) by a factor k is to scale each inductance and capacitance by the same
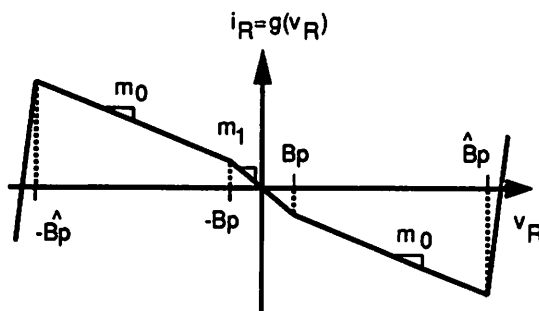
Figure 3: Every physically realizable nonlinear resistor N_R is eventually passive — the outermost segments (while not necessarily linear as shown here) must lie completely within the first and third quadrants of the $v - i$ plane for sufficiently large $|v|$ and $|i|$.

factor k; resistances are unaffected by a time scaling. In particular, slowing time by 2×10^4 decreases C_1, C_2, and L by the same factor. The revised parameters are now:

$$
\begin{aligned}
C_1 &= 1/18 \times 10^{-7}\text{F} &= 5.56\text{nF} \\
C_2 &= 1/2 \times 10^{-7}\text{F} &= 50\text{nF} \\
L &= 1/14 \times 10^{-1}\text{H} &= 7.14\text{mH} \\
G &= 0.7 \times 10^{-3}\text{S} &= 0.7\text{mS (which corresponds to } R = 1428\Omega)
\end{aligned}
$$

The breakpoints and slopes of the piecewise-linear resistor N_R are unchanged when time is rescaled.

These are the component values which Matsumoto et al. used to confirm their computer simulations experimentally [MCK85]. This will be our starting point too, but with a slight difference. Electronic components are available "off-the-shelf" in standard values; 7.14 mH, 5.56 nF, 50 nF, and 1428 Ω are not standard values. Therefore, we arbitrarily choose 18 mH, 10 nF, 100 nF, and 1800 Ω as a nearby "standard value" starting point.

Having scaled current and time, our next goal is to construct the Chua diode: a nonlinear resistor with the $v - i$ characteristic shown in Fig. 2. The important feature of this is that it possesses two negative slopes m_0 and m_1.

In order to understand the design methodology presented here, we first review some results from nonlinear circuit theory.

Eventual passivity

By definition, the Double Scroll attractor is bounded. This is important because all physical resistors are *eventually passive*, meaning simply that for a large enough voltage across its terminals, the power $P\ (= vi)$ consumed by a real resistor is positive. For large enough $|v|$ or $|i|$, therefore, the characteristic must lie only in the first and third quadrants of the $v - i$ plane. Hence, any physical realization of the three-segment characteristic specified in Chua's circuit must include at least two more segments which return the characteristic to the first and third quadrants (see Fig. 3). As long as the voltages and currents on the attractor are restricted to the negative resistance region of the characteristic, these outer segments will not affect the circuit's behavior. In our discussion of a practical implementation of a Chua diode, we will show how to maximize the extent of the negative resistance regions.

3 Negative resistance converters

There are many ways to synthesize a negative resistance, one of which is by connecting three positive linear resistors to a voltage-controlled voltage source to form a negative resistance converter. This arrangement is attractive from an experimentalist's point of view because it is readily implemented by means of an operational amplifier (op amp).
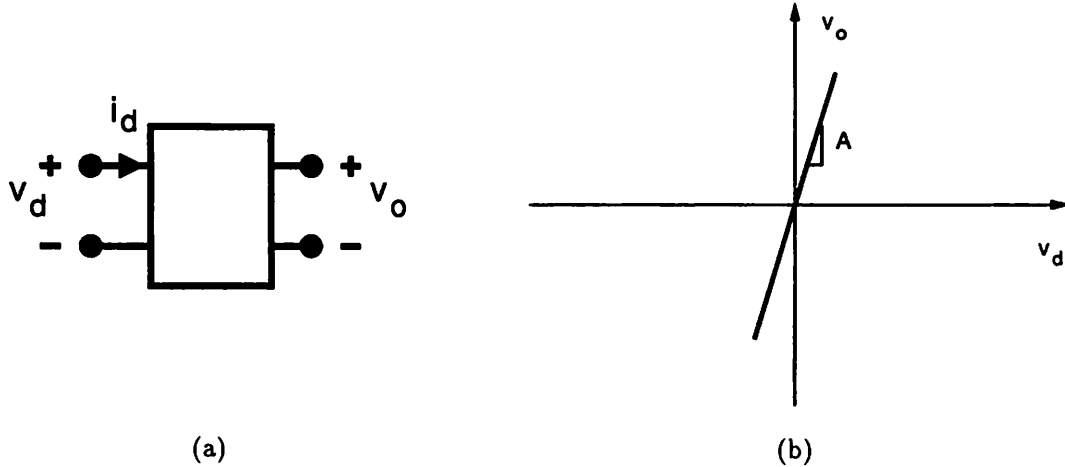
4

Figure 4: (a) Voltage-Controlled Voltage Source (VCVS): $i_d = 0$ and $v_o = f(v_d)$; (b) voltage transfer characteristic of linear VCVS with gain A.

Voltage-controlled voltage source (VCVS)

A voltage-controlled voltage source (VCVS) is an ideal circuit element which has two input terminals and two output terminals (see Fig. 4(a)). It is characterized by two properties: no current flows into or out of the input terminals, and the voltage v_o which appears across the output terminals is a function of the potential difference v_d between the input terminals. The simplest non-trivial functional relation between the output and input voltages of a VCVS occurs when v_o depends linearly on v_d, i.e. $v_o = Av_d$. This is illustrated in Fig. 4(b).

VCVS-based negative resistance converter

A two-terminal negative resistance converter can now be produced by connecting three positive resistances around a voltage-controlled voltage source as shown in Fig. 5(a).

Let us assume that the VCVS in Fig. 5(a) is linear with voltage transfer function $v_o = Av_d$. When A is sufficiently large, this negative resistance converter has the following $v - i$ relation (which is derived in Appendix A):

$$i = -\frac{R_2}{R_1 R_3} v$$

By choosing $R_2 = R_1$, this reduces to:

$$i = -\frac{1}{R_3} v$$

Thus, looking between the input terminals of this element N_R, one sees a resistance of $-R_3$.

Operational amplifiers

An operational amplifier (op amp) provides us with a real-world approximation to a voltage-controlled voltage source.

Consider the circuit shown in Fig. 6(a), which consists of an operational amplifier and its associated power supplies V^+ and V^- (depicted as batteries). A voltage applied between the non-inverting and inverting input terminals (labeled "+" and "−") produces a potential difference between the output terminal and the reference terminal (usually the common point of the power supplies).[1]

---

[1] We consider only the case when the voltages at the non-inverting and inverting terminals relative to the reference terminal are within the common-mode range of the op amp.

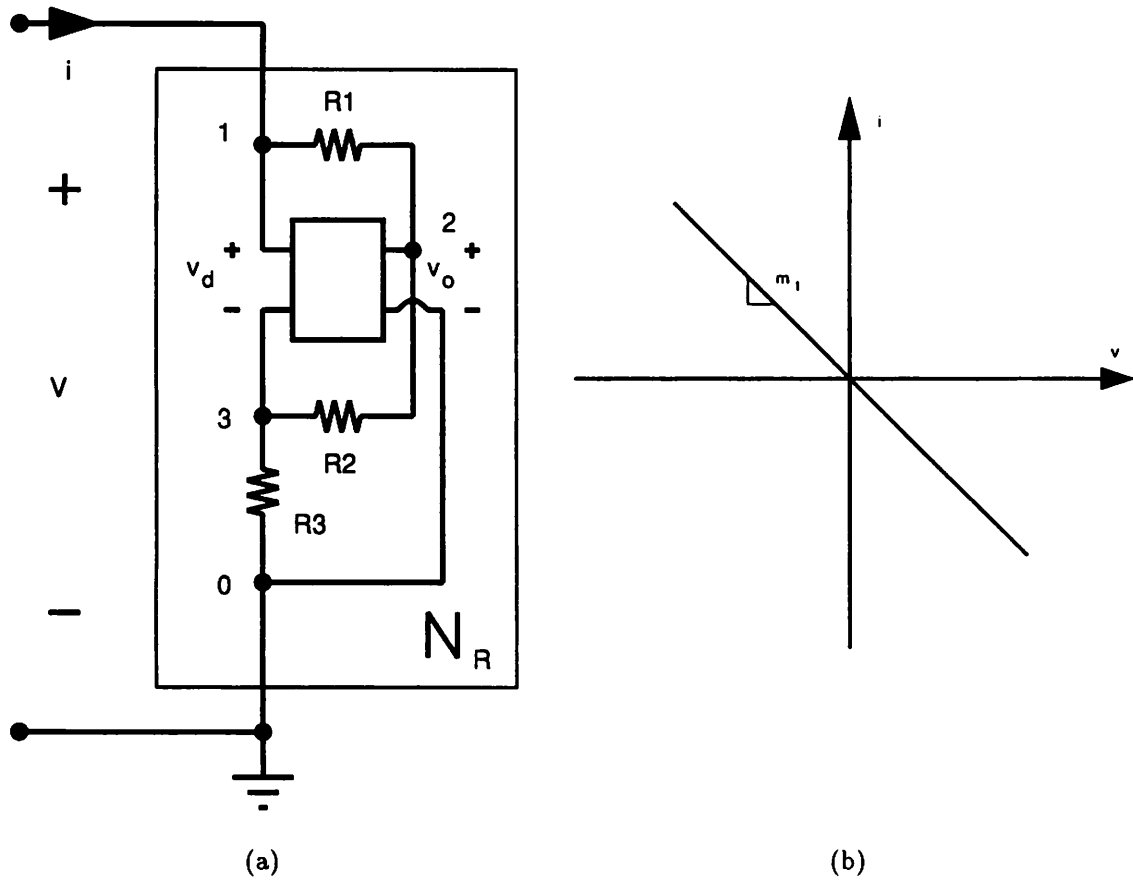(a)   (b)

Figure 5: (a) Negative resistance converter using a voltage-controlled voltage source; (b) $v - i$ characteristic of negative resistance converter using a VCVS with linear voltage transfer function $v_o = A v_d$. The slope of the $v - i$ characteristic is given by $m_1 = \frac{(1-A)R_2+R_3}{R_1[R_2+(1+A)R_3]}$; for sufficiently large A, $i \approx -\frac{R_2}{R_1 R_3} v$.
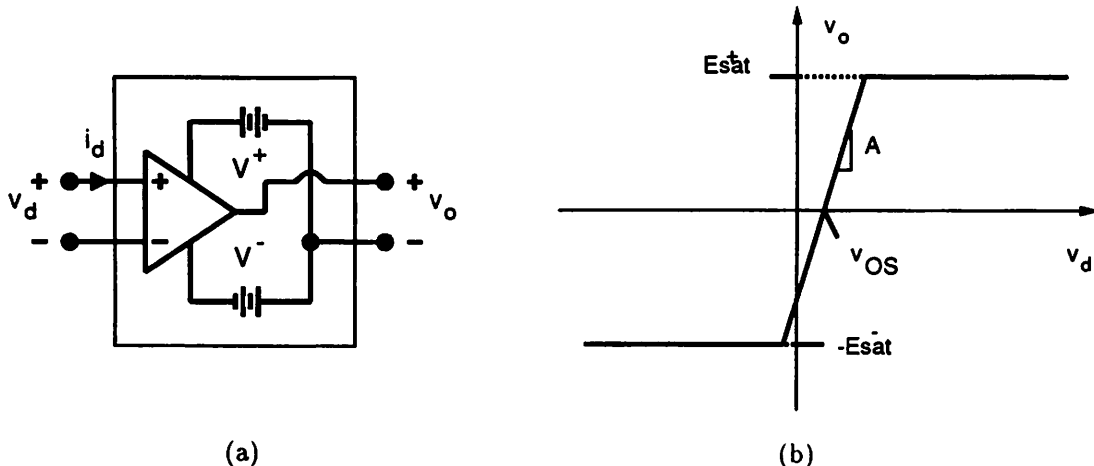
6

Figure 6: (a) Operational amplifier with associated power supplies; (b) Voltage transfer characteristic of op amp.

This real op-amp-and-batteries circuit module draws a small current i_d at its input terminals; let us assume that $i_d = 0$.

When the differential input voltage v_d of a real op amp is sufficiently large in magnitude and negative, the output is approximately constant at $-E_{sat}^-$; this is called the *negative saturation region*. When the input is small in magnitude, the output varies almost linearly with the input; this is called the *linear region*. The gain in the linear region is usually greater than 10^5V/V. In addition, the characteristic is offset from the origin by an input offset voltage v_{OS}, which is typically a few mV. When the input voltage is large and positive, the output assumes a maximum value of E_{sat}^+; this is called the *positive saturation region*. The DC voltage transfer function of a real op amp is thus closely approximated by a three-segment piecewise-linear characteristic, as shown in Fig. 6(b).

Because a real op amp contains compensation and parasitic capacitances, a complete model of the device should include dynamic elements. We assume here that the op amp behaves purely resistively at the frequencies of interest in Chua's circuit. This can always be ensured by appropriately scaling time as indicated in section 2. Thus, we neglect all frequency-dependent effects in the op amp and treat it as purely resistive.

We assume too that the output impedance of the op amp is sufficiently small that it can be neglected.

Thus, for our purposes, the output of the op amp looks like an ideal voltage source and its input looks like an open circuit. We can therefore model the op amp by a VCVS: $i_d = 0; v_o = f(v_d)$, where $f(\cdot)$ is as shown in Fig. 6(b).

The advantage of this piecewise-linear model is that we can now determine the behavior of a circuit containing op amps and other components by analyzing each linear region of operation (negative saturation, linear, and positive saturation) separately. For further discussion and worked examples of op amp circuits using piecewise-linear techniques, see [CDK87] and [KC91].

Negative resistance converter using an op amp

We can now build a negative resistance converter using an op amp as shown in Fig. 7(a). The driving point $(v - i)$ characteristic is shown in Fig. 7(b) (See Appendix B for the details of the calculation).

The $v - i$ relation is piecewise-linear and consists of three segments. As before, we assume that A is large. The central portion then has slope $m_1 \approx -R_2/(R_1 R_3)$ and the outer regions (corresponding to saturation of the op amp—a consequence of eventual passivity) have slopes $m_0 = 1/R_1$. If we set $R_2 = R_1$ then $m_1 = -1/R_3$.

In the following, we assume that the saturation levels of the op amp are equal in magnitude and that the offset v_{OS} is zero. Later, we will discuss techniques for accomplishing this. Thus, $E_{sat}^+ = E_{sat}$ and

(a)   (b)
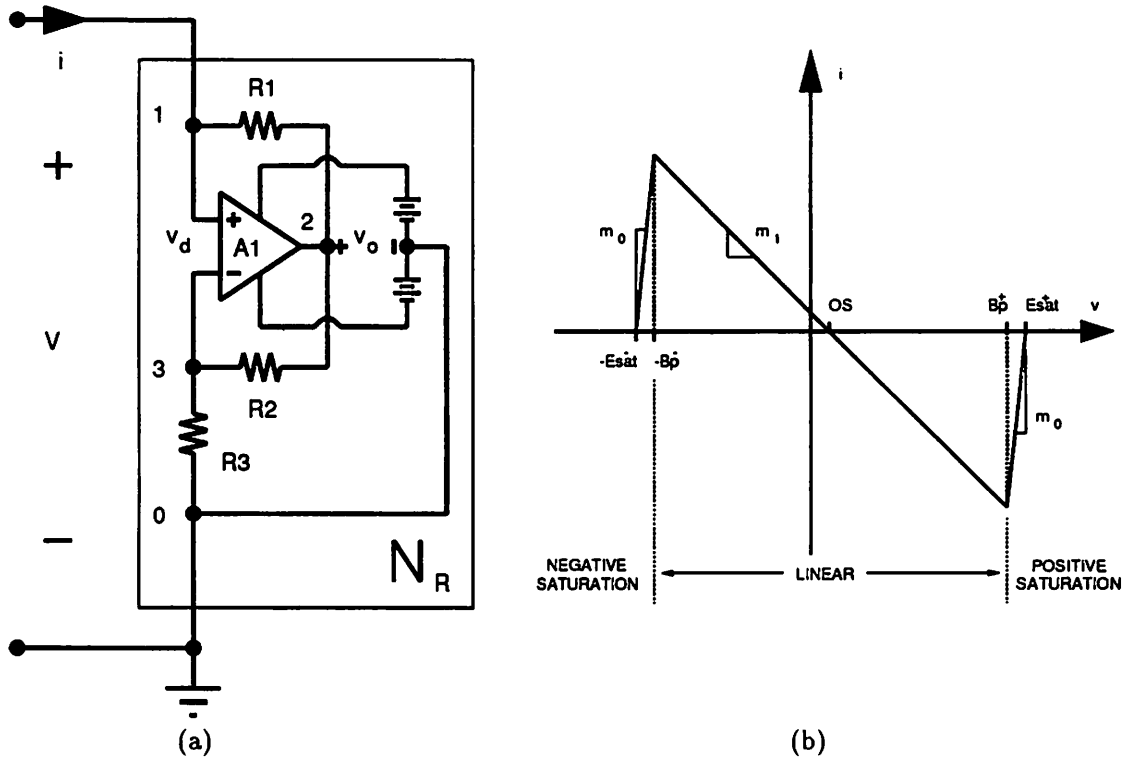
Figure 7: (a) Operational amplifier-based negative resistance converter; (b) $v - i$ characteristic of op amp negative resistance converter, assuming the three-segment piecewise-linear voltage transfer characteristic in Fig. 6(b). $m_0 = \frac{1}{R_1}$, $B_P^+ = \frac{R_2+(1+A)R_3}{A(R_2+R_3)} E_{sat}^+ + v_{OS}$, $m_1 = \frac{(1-A)R_2+R_3}{R_1[R_2+(1+A)R_3]}$, $-B_P^- = -\frac{R_2+(1+A)R_3}{A(R_2+R_3)} E_{sat}^- + v_{OS}$, and $OS = -\frac{A(R_2+R_3)}{(1-A)R_2+R_3} v_{OS}$. When the offset v_{OS} is reduced to zero, the gain A is large, and $R_2 = R_1$, then $m_0 = \frac{1}{R_1}$, $B_P^+ \approx \frac{R_3}{R_2+R_3} E_{sat}^+$, $m_1 \approx -\frac{R_2}{R_1 R_3}$, $-B_P^- \approx -\frac{R_3}{R_2+R_3} E_{sat}^-$, and $OS = 0$.
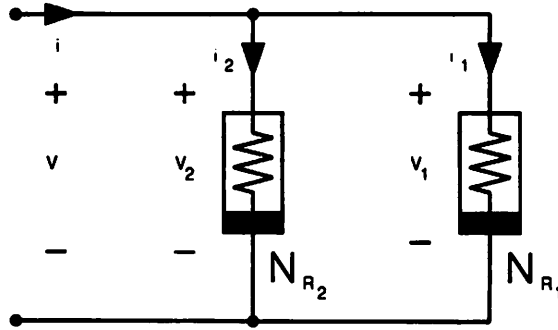
8

Figure 8: Parallel connection of two nonlinear resistors. If $i_1 = f_1(v_1)$ and $i_2 = f_2(v_2)$, then $i = f_1(v) + f_2(v)$.

$-E_{sat}^- = -E_{sat}$, by assumption, and the breakpoints occur at $\pm[R_3/(R_2 + R_3)]E_{sat}$.

The op amp negative resistance converter (NRC) will be the core building block for the nonlinear resistor in Chua's circuit. What happens if we now connect two such NRCs in parallel [CDK87]?

4 Putting the blocks together

Two nonlinear resistors are connected in parallel, as shown in Fig. 8. Let us assume that both are voltage-controlled. The current i_1 which flows in the two-terminal resistor N_{R_1}, when a voltage v_1 is applied across its terminals, is defined by $i_1 = f_1(v_1)$. Similarly, a current $i_2 = f_2(v_2)$ flows in N_{R_2}. The total current flowing into the pair is given by $i = g(v)$ where $g(v) = f_1(v) + f_2(v)$. Thus, the parallel combination of two (or more) voltage-controlled nonlinear resistors is also a voltage-controlled nonlinear resistor.

We can determine the shape of $g(\cdot)$ graphically by adding i_1 and i_2 for each v, as indicated in Fig. 9. The process is simplified considerably if the constituent functions $f_1(\cdot)$ and $f_2(\cdot)$ are piecewise-linear. For more extensive discussion of series and parallel combinations of nonlinear resistors, see [CDK87].

It should now be clear how a five-segment physically realizable piecewise-linear resistor of the type needed in Chua's circuit can be constructed simply by connecting in parallel two negative resistance converters with appropriately shaped $v - i$ characteristics.

5 Realization of the Chua diode for Chua's circuit using two op amp negative resistance converters

Fig. 10 shows an op amp implementation of Chua's circuit. The desired Chua diode $v - i$ characteristic is produced by connecting two voltage-controlled negative resistance converters N_{R1} and N_{R2} in parallel. Nonlinear resistor N_{R_1} has a three-segment piecewise-linear characteristic with slopes m_{01} and m_{11} and breakpoints $\pm B_{P1}$ (as in Fig. 9(b)). Similarly, N_{R_2} has slopes m_{02} and m_{12} and breakpoints $\pm B_{P2}$ (Fig. 9(a)). The compound five-segment characteristic has slopes m_{-1}, m_0, and m_1 and two pairs of breakpoints at $\pm B_{P1}$ and $\pm B_{P2}$ (as in Fig. 9(c)).

We have seen from our discussion of the op amp negative resistance converter that specifying $R_2 = R_1$ in Fig. 7(a) yields slopes R_1 and $-1/R_3$, with breakpoints at $\pm[R_3/(R_2 + R_3)]E_{sat}$.

Thus, with $R_2 = R_1$,

$$m_{01} = \frac{1}{R_1}$$
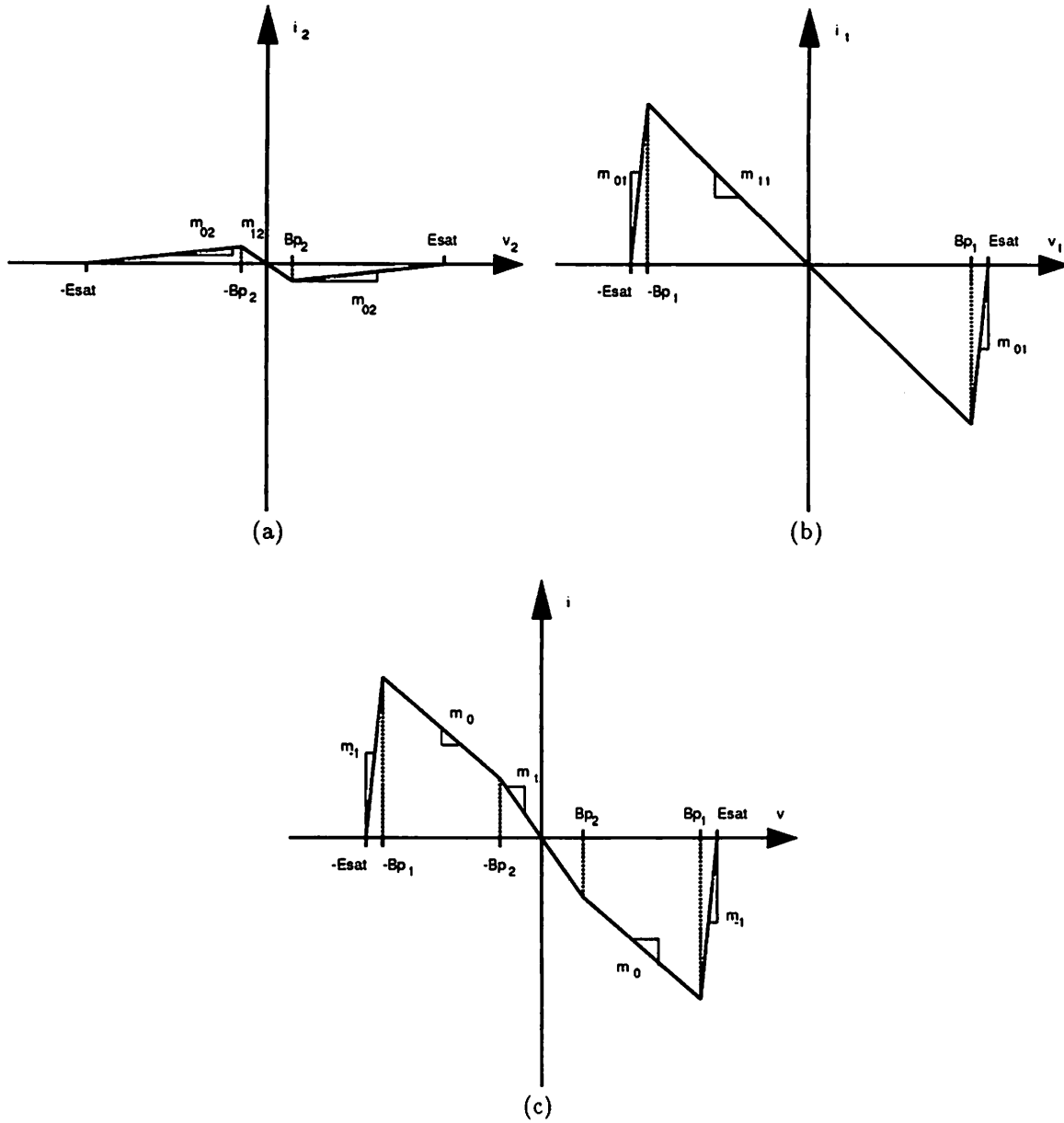
$$m_{11} = -\frac{1}{R_3}$$

9

Figure 9: Graphical combination of piecewise-linear voltage-controlled resistors: (a) $v - i$ characteristic of N_{R2}; (b) $v - i$ characteristic of N_{R1}; (c) $v - i$ characteristic of N_{R2} in parallel with N_{R1}.
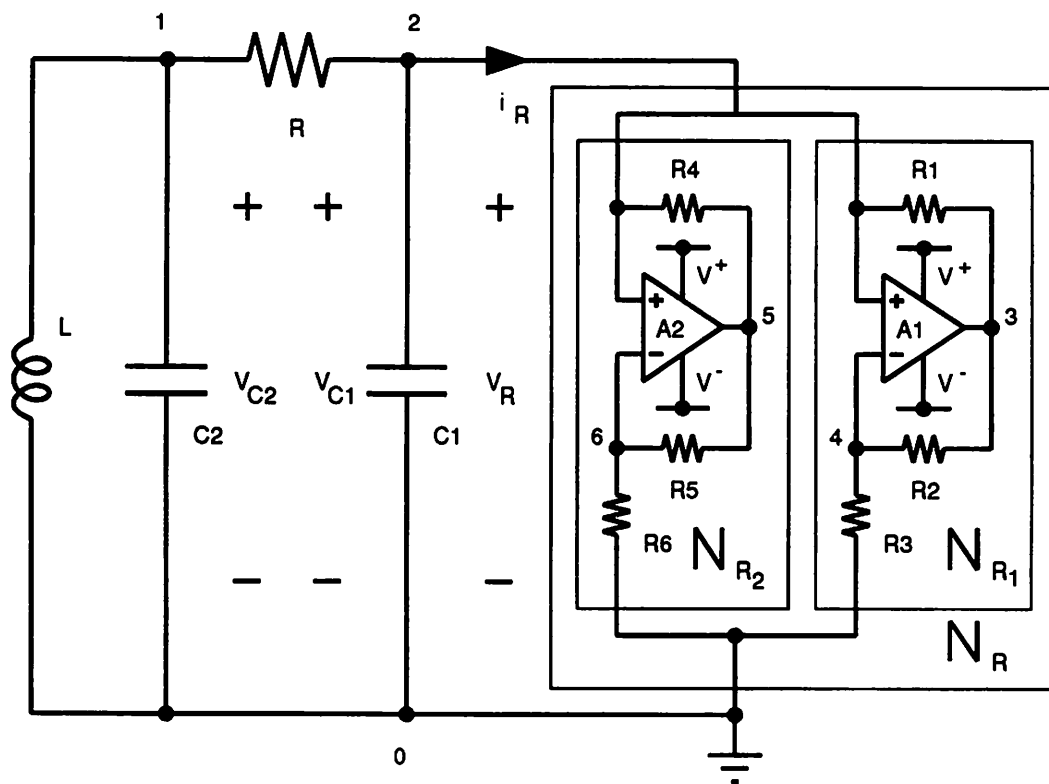
Figure 10: Realization of Chua's circuit using two op amps and six linear resistors to implement the Chua diode N_R. The two op amps are available in a single eight-pin dual in-line package (DIP).

$$B_{P1} = \frac{R_3}{R_2 + R_3} E_{sat}$$

Similarly, $R_5 = R_4$ gives

$$m_{02} = \frac{1}{R_4}$$

$$m_{12} = -\frac{1}{R_6}$$

$$B_{P2} = \frac{R_6}{R_5 + R_6} E_{sat}$$

From graphical considerations of the compound characteristic, we have:

$$m_{11} + m_{02} = m_0$$

$$m_{11} + m_{12} = m_1$$

With these observations, we can derive a design strategy for determining the appropriate values of the components R_1–R_6 from m_0, m_1, and B_{P2}. The method is developed in Appendix C.

Design procedure

E_{sat} is determined by the power supplies and internal structure of the op amps. We do not necessarily know its value a priori but it can be measured. The shape of the desired characteristic determines B_{P2}, m_0, and m_1. We are free to choose B_{P1} or m_{-1}.

- Choose R_1 large enough that it will not significantly load the op amp (say 330 Ω). Calculate $B_{P1} = E_{sat}/(1 - m_1 R_1)$. If B_{P1} is not large enough that the dynamics of the attractor will remain within the negative-resistance region of the characteristic, reduce R_1 and try again. One must trade off the length of the negative resistance region and the size of R_1.

- Choose $R_2 = R_1$.

- Evaluate

$$R_3 = \frac{E_{sat}}{(B_{P2} - E_{sat})m_0 - B_{P2}m_1}$$

- Calculate

$$R_4 = \frac{E_{sat}}{B_{P2}(m_0 - m_1)}$$

- Set $R_5 = R_4$.

- Evaluate

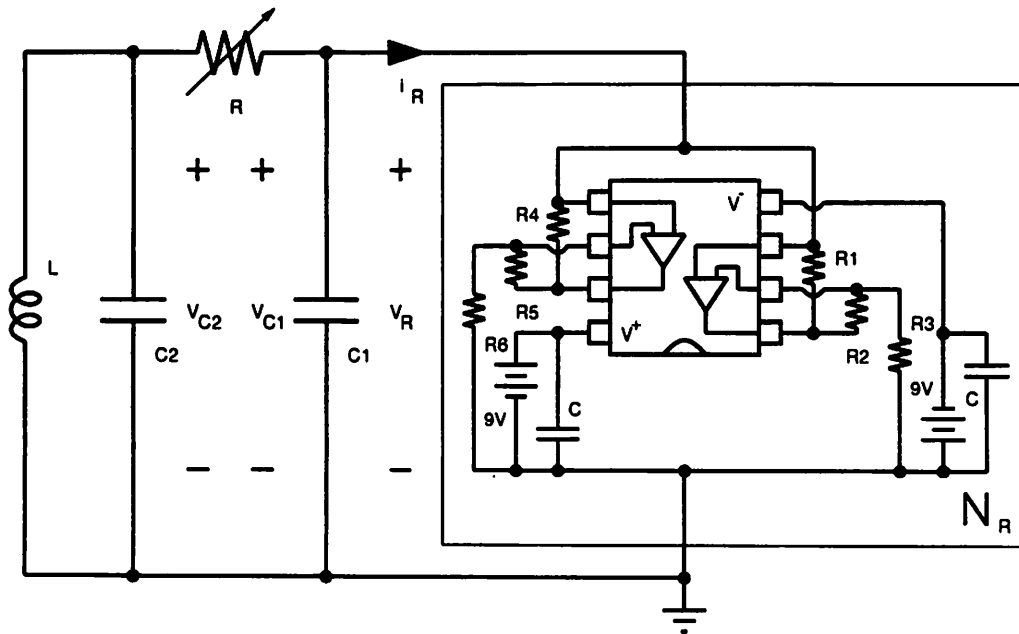$$R_6 = \frac{E_{sat}}{(E_{sat} - B_{P2})(m_0 - m_1)}$$

12

Figure 11: Practical realization of Chua's circuit using an eight-pin dual op amp integrated circuit.

Practical implementation of Chua's circuit—worked example

Fig. 11 shows a practical implementation of Chua's circuit using an Analog Devices AD712 dual BiFET op amp, two 9V batteries, and six resistors to implement the Chua diode.

Using two 9V batteries to power the op amps gives $V^+ = 9$ V and $V^- = -9$ V. From measurements of the saturation levels of the AD712 outputs, $E_{sat} \approx 8.3$ V. The desired nonlinear characteristic is defined by $m_0 = -0.409$ mS, $m_1 = -0.756$ mS, and $B_{P2} = 1.08$ V. Our slopes and breakpoints are chosen (with hindsight) to be slightly different from those used by Matsumoto et al. [MCK85] because we wish to use only off-the-shelf components in this example.

Following the design strategy above, we derive a complete component list for this circuit. In addition to the components listed, we recommend that a bypass capacitor C of at least 0.1μF be connected across each power supply, as shown in Fig. 11, as close to the op amp as possible. The purpose of these capacitors is to maintain the power supplies at a constant DC voltage.

13

Component list

Element	Description	Value	Tolerance
A_1	Op amp ($\frac{1}{2}$ AD712, TL082, or equivalent)		
R_1	$\frac{1}{4}$W Resistor	220 Ω	$\pm 5\%$
R_2	$\frac{1}{4}$W Resistor	220 Ω	$\pm 5\%$
R_3	$\frac{1}{4}$W Resistor	2.2 kΩ	$\pm 5\%$
A_2	Op amp ($\frac{1}{2}$ AD712, TL082, or equivalent)		
R_4	$\frac{1}{4}$W Resistor	22 kΩ	$\pm 5\%$
R_5	$\frac{1}{4}$W Resistor	22 kΩ	$\pm 5\%$
R_6	$\frac{1}{4}$W Resistor	3.3 kΩ	$\pm 5\%$
C_1	Capacitor	10 nF	$\pm 5\%$
R	Potentiometer	2 kΩ	
C_2	Capacitor	100 nF	$\pm 5\%$
L	Inductor (TOKO type 10RB or equivalent)	18 mH	$\pm$ 10%

Table 1: Component list for robust implementation of Chua's circuit. See Fig. 11.

Experimental verification of the Chua diode $v - i$ characteristic

The $v - i$ characteristic of the Chua diode N_R can be measured in isolation by means of the circuit shown in Fig 12.

Resistor R_S, known as a current-sensing resistor, is used to measure the current i_R which flows into the Chua diode N_R when a voltage v_R is applied across its terminals. An appropriate choice of R_S in this example is 100 Ω. Current i_R flowing in R_S then causes a voltage $v_{i_R} = -100 i_R$ to appear across the sensing resistor. Thus, we can measure the $v - i$ characteristic of N_R by applying a voltage v_S as shown and plotting $v_{i_R} (\propto -i_R)$ versus v_R. This is achieved by connecting v_{i_R} to the Y-input and v_R to the X-input of an oscilloscope in X-Y mode. The resulting characteristic for the components listed in the table is shown in Fig 13. Note that we have plotted $-v_{i_R}$ versus v_R; this is possible if your oscilloscope permits inversion of the Y-input in X-Y mode.

6 Bifurcations and chaos

R bifurcation sequence

By reducing the variable resistor R in Fig. 11 from 2000 Ω towards zero, Chua's circuit exhibits a sequence of bifurcations from DC equilibrium through a Hopf bifurcation and period-doubling sequence to a Rössler-type attractor and the Double Scroll strange attractor, as illustrated in Fig. 14. A two-dimensional projection of the attractor is obtained by connecting v_{C_1} and v_{C_2} to the X and Y channels, respectively, of an X-Y oscilloscope.

Notice that varying R in this way causes the size of the attractors to change: the period-one orbit is large, period-two is smaller, the Rössler-type attractor is smaller again, and the Double Scroll shrinks considerably
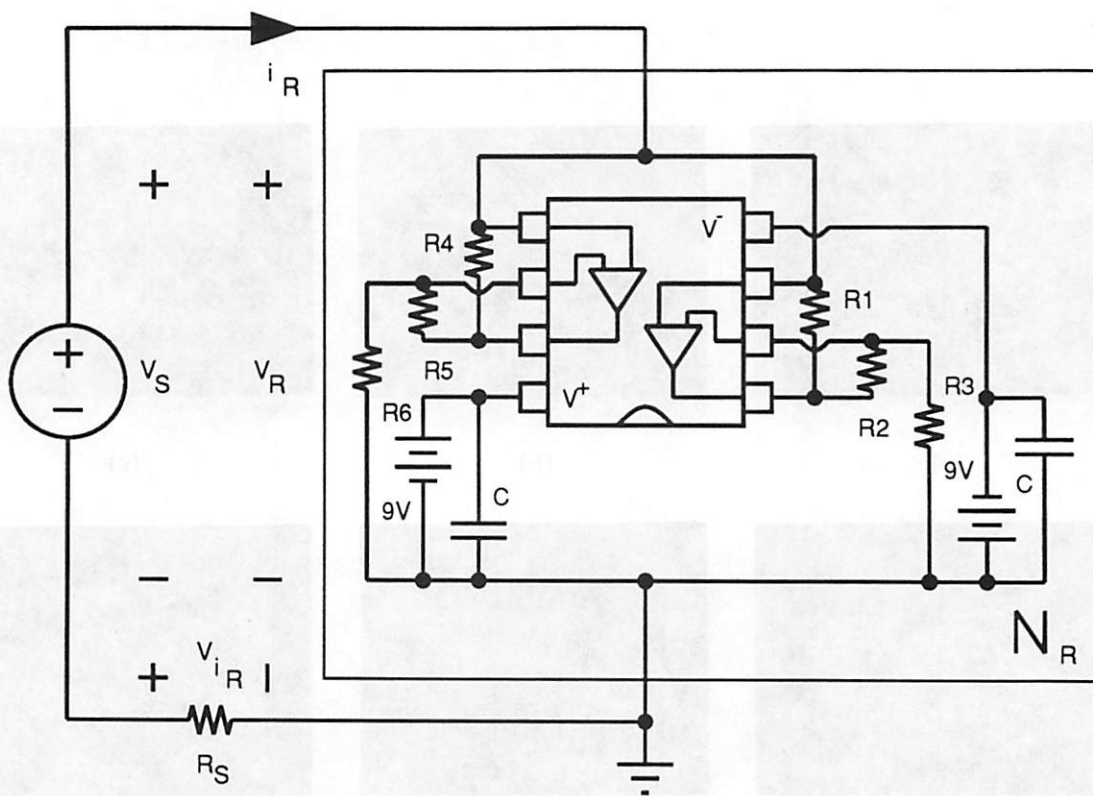
Figure 12: The $v - i$ characteristic of Chua diode N_R can be measured by applying a triangular voltage waveform v_S to the series combination of N_R and a small current-sensing resistor R_S. Plot $-v_{i_R}(\propto i_R)$ versus v_R. The eight-pin dual op amp package is shown from above in schematic form. The reference end of the package is indicated by a dot or a semicircle (shown here).
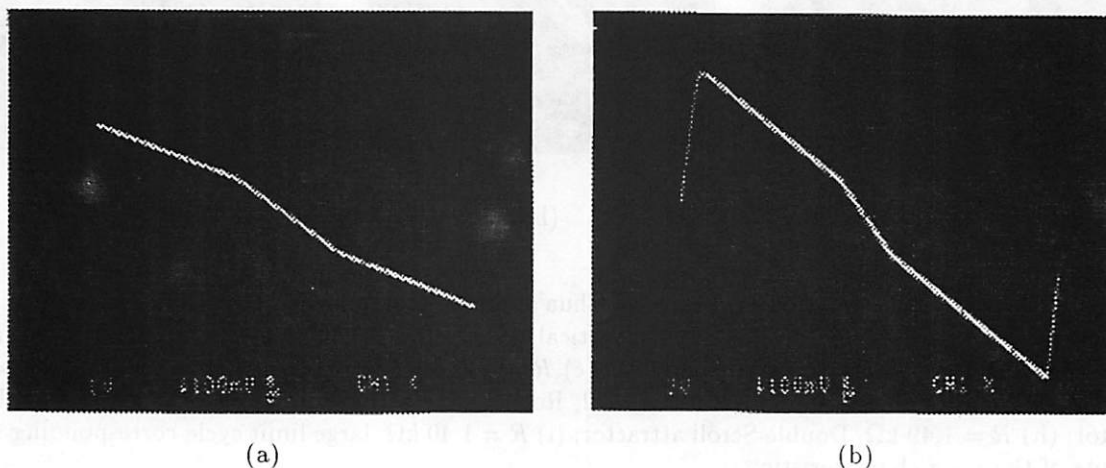

Figure 13: Measured $v - i$ characteristic of the Chua diode. (a) v_S is a triangular waveform with zero DC offset, amplitude 7V peak-to-peak, and frequency 30 Hz. Horizontal axis: v_R (1V/div); Vertical axis: $-v_{i_R}$ (100mV/div); (b) v_S is a triangular waveform with zero DC offset, amplitude 15V peak-to-peak, and frequency 30 Hz. Horizontal axis: v_R (2V/div); Vertical axis: $-v_{i_R}$ (100mV/div).
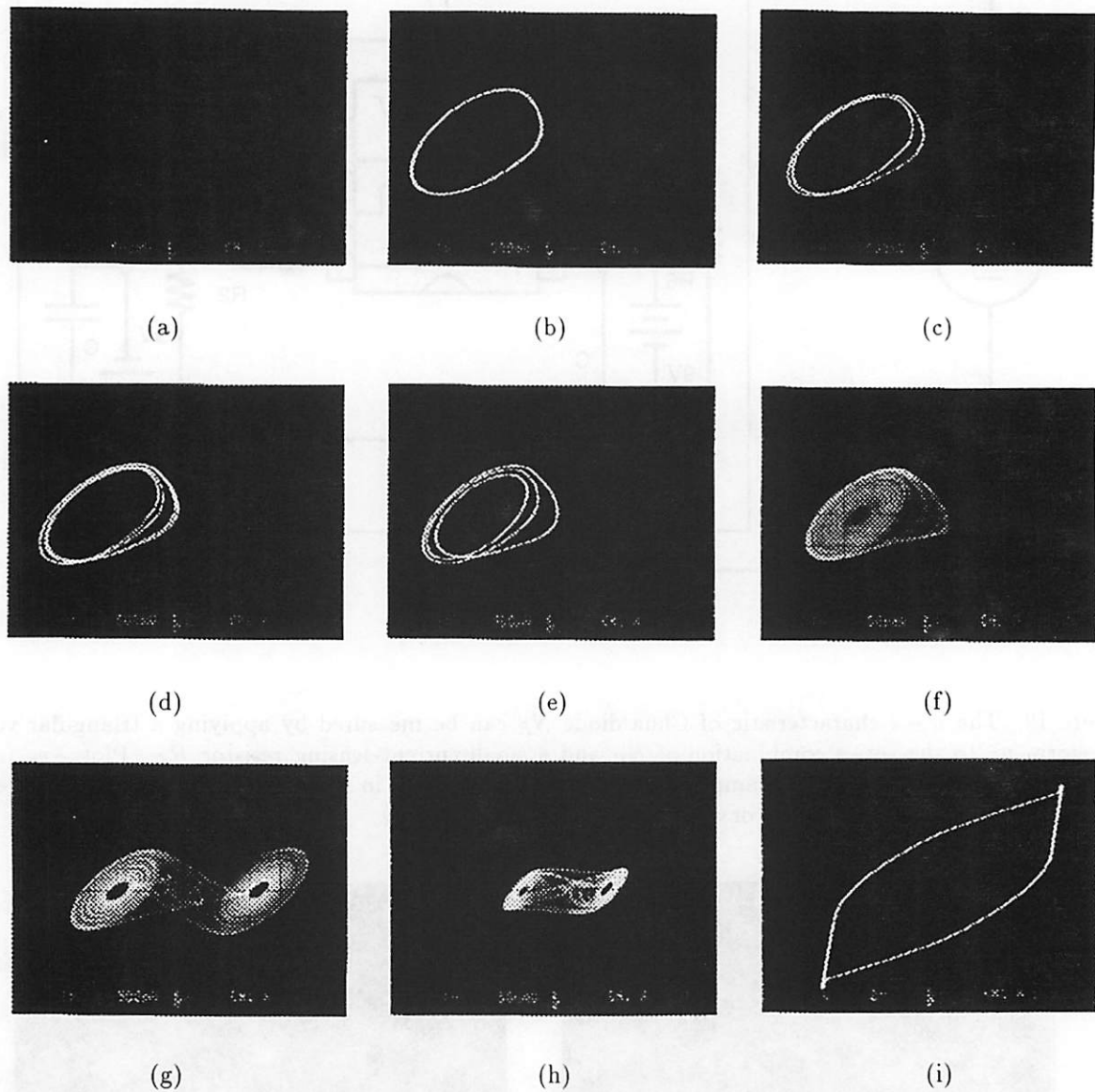
(a)   (b)   (c)

(d)   (e)   (f)

(g)   (h)   (i)

Figure 14: Typical R bifurcation sequence in Chua's circuit (component values as in the table above). Horizontal axis v_{C_1} (a)–(h) 1V/div, (i) 2V/div; vertical axis v_{C_2} (a)–(h) 500mV/div, (i) 2V/div. (a) $R = 2.00$ kΩ, DC equilibrium; (b) $R = 1.88$ kΩ, period-1; (c) $R = 1.85$ kΩ, period-2; (d) $R = 1.84$ kΩ, period-4; (e) $R = 1.825$ kΩ, period-3 window; (f) $R = 1.79$ kΩ, Rössler-type attractor; (g) $R = 1.74$ kΩ, Double Scroll attractor; (h) $R = 1.49$ kΩ, Double Scroll attractor; (i) $R = 1.40$ kΩ, large limit cycle corresponding to outer segments of the $v - i$ characteristic.

16

before it dies.

C_1 bifurcation sequence

An alternative way to view the bifurcation sequence is by adjusting C_1. In this case, fix the value of R at 1800 Ω and vary C_1. Monitor v_{C_1} and v_{C_2} as before. The full range of bifurcations from equilibrium through Hopf, period-doubling, Rössler, and Double Scroll can be observed as C_1 is reduced from 12.0 nF to 6.0 nF (see Fig. 15). In contrast to the R bifurcation sequence, the size of the Double Scroll attractor remains almost constant here.

7 Simulation of Chua's circuit

These experimental observations may be confirmed by simulation using a specialized Nonlinear Dynamics simulation package such as INSITE [PC87b]. Alternatively, one can simulate Chua's circuit on a general-purpose circuits simulator such as SPICE.

SPICE simulations

The op amps in our realization of the circuit may be modeled using macro-model subcircuits which are available from a number of integrated circuits manufacturers. Analog Devices' macro-models [Ana91] are compatible with SPICE release 2G6 and later while Texas Instruments [Tex90] use PSpice [Ras90] polynomial controlled sources which are incompatible with Berkeley SPICE [JQN+91].

Three attractors in the C_1 bifurcation sequence were simulated using SPICE 3d2 with the input deck shown in Fig. 16; the results are shown in Fig. 17. The AD712 op amp [Ana90] is modeled with Analog Devices' AD712 SPICE macro-model [Ana91]. A real inductor has a non-zero series resistance which we have included in the SPICE model; we measured RL = 13.5Ω. Node numbers are as in Fig. 10. The power rails are 111 and 222; 10 is the "internal" node of our physical inductor where its series inductance is connected to its series resistance.

We note in passing that the principal difference between the R and C_1 bifurcation sequences is that while the size of the Double Scroll attractor varies considerably with R, adjusting C_1 has little effect on its magnitude.

8 Effects of non-idealities on Chua's circuit

In our discussion of the SPICE model, we introduced a small parasitic series resistor to account for the DC resistance of a physical inductor. The effect of this parasitic is small.

In contrast, non-idealities in the op amp have a major effect so it is important to be aware of these influences. We noted earlier that the outer regions of the $v - i$ characteristic have no effect on the shape of the attractor if the voltages and currents on the attractor remain sufficiently small. If the attractor grows too large in magnitude, it will be at best be clipped. This effect is illustrated in Fig. 18. By reducing the value of C_1 from 10 nF to 8 nF, the amplitude of the attractor in the R bifurcation sequence grows too large and is clipped.

The breakpoints in the nonlinear resistor's $v - i$ characteristic are proportional to the saturation levels of the op amps. The saturation levels in turn are determined by the power supply voltages and by the internal architecture of the op amps. If the levels are different, as they typically are, the resulting $v - i$ characteristic will be asymmetric. This results in a Double Scroll attractor which has one lobe bigger than the other; the effect is illustrated in Fig. 19. Here, we have reduced the negative power supply voltage from 9V to 7V in magnitude. The result is to move the left breakpoint of the $v - i$ characteristic, which in turn produces an asymmetry in the attractor.

We also saw that the input offset voltage v_{OS} of an op amp causes a shift in the $v - i$ characteristic when it is used as a negative resistance converter (refer back to Fig. 7(b)). While asymmetry may be aesthetically unpleasing, it has little effect on the bifurcation sequence or on the nature of the attractor.
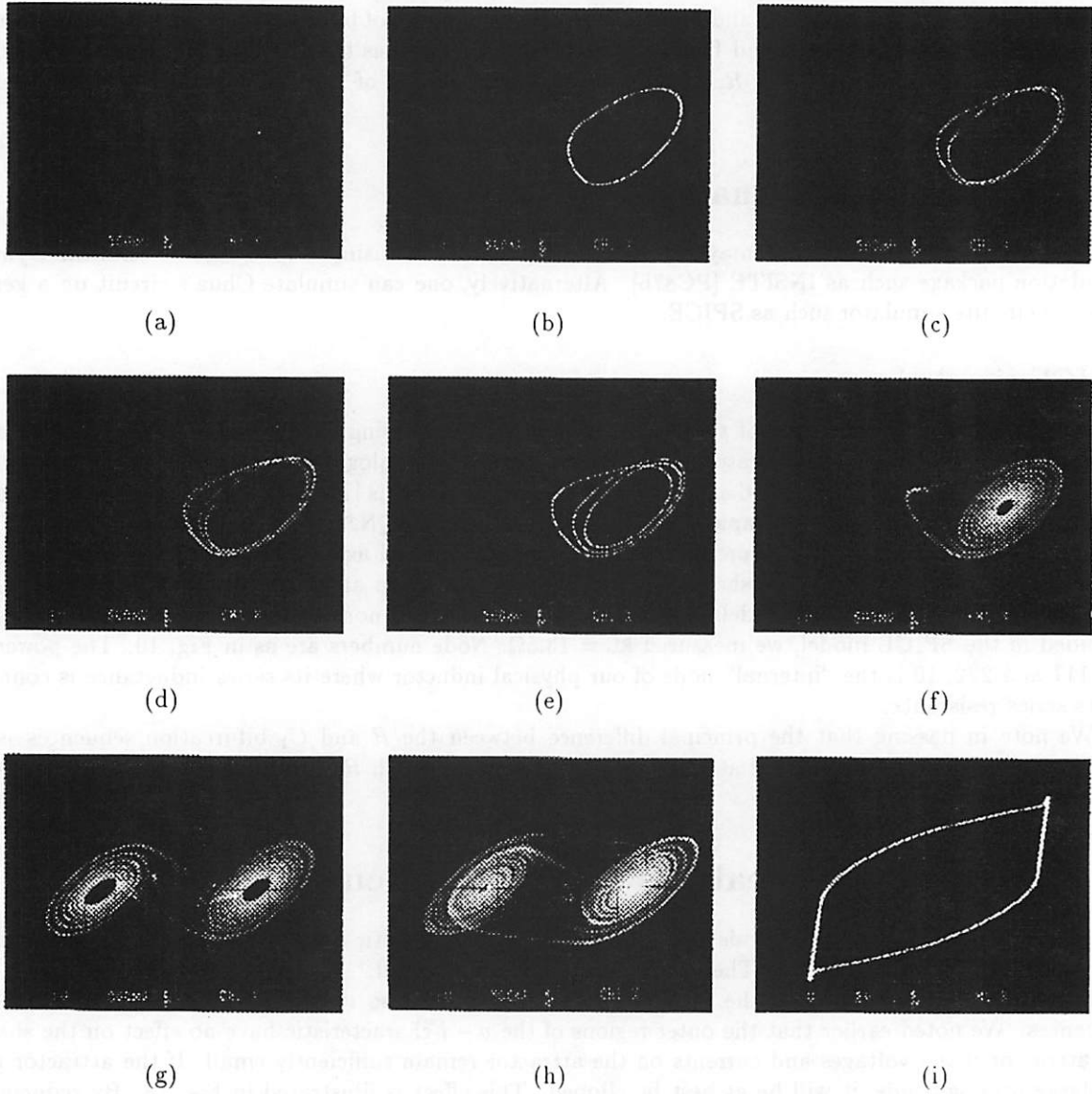
Figure 15: Typical C_1 bifurcation sequence in Chua's circuit (component values as shown in the table above [R = 1800 Ω]). Horizontal axis v_{C_1} (a)–(h) 1V/div, (i) 2V/div; vertical axis v_{C_2} (a)–(h) 500mV/div, (i) 2V/div. (a) $C_1 = 11.0$ nF, DC equilibrium; (b) $C_1 = 10.2$ nF, period-1; (c) $C_1 = 10.1$ nF, period-2; (d) $C_1 = 10.0$ nF, period-4; (e) $C_1 = 9.91$ nF, period-3 window; (f) $C_1 = 9.7$ nF, Rössler-type attractor; (g) $C_1 = 9.4$ nF, Double Scroll attractor; (h) $C_1 = 8.0$ nF, Double Scroll attractor; (i) $C_1 = 7.0$ nF, large limit cycle corresponding to outer segments of the $v - i$ characteristic.

18

```
MODEL1

V+   111  0     DC  9
V-   0    222   DC  9

L    1    10    0.018
RL   10   0     13.5
R    1    2     1800
C2   1    0     100.0N
C1   2    0     10.0N

XA1  2 4 111 222 3 AD712
R1   2 3   220
R2   3 4   220
R3   4 0   2200

XA2  2 6 111 222 5 AD712
R4   2 5   22000
R5   5 6   22000
R6   6 0   3300

*
* The AD712 SPICE Macro-model is available from Analog Devices, Inc.
*

.WIDTH OUT=80
.IC V(2)=2.0 V(1)=0
.TRAN 0.01MS 100.0MS 80.0MS
.PRINT TRAN V(2) V(1)
.PLOT  TRAN V(2) V(1)
.END
```

Figure 16: SPICE deck to simulate the transient response of our dual op amp implementation of Chua's circuit. Node numbers are as in Fig. 10. The op amps are modeled by the AD712 macro-model from Analog Devices. RL models the series resistance of the real inductor L.
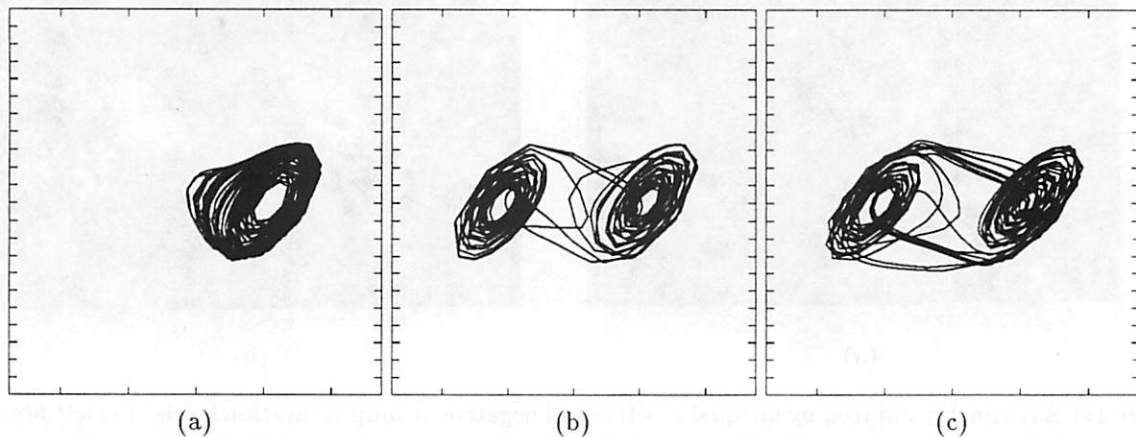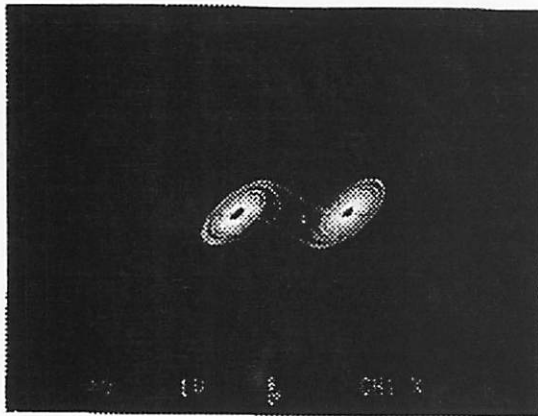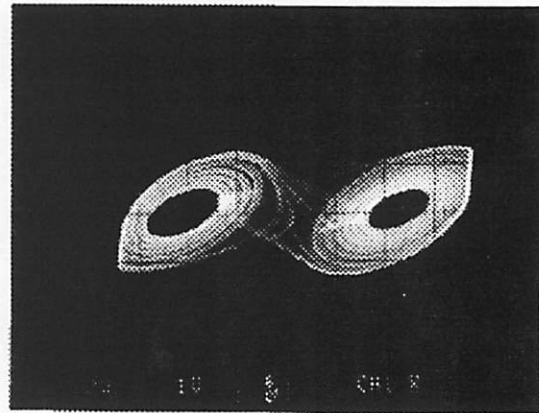

(a)   (b)   (c)

Figure 17: Attractors in Chua's circuit from SPICE 3d2 simulations of the C_1 bifurcation sequence. Horizontal axis v_{C_1} 2V/div; vertical axis v_{C_2} 200mV/div. (a) $C_1 = 10.1$ nF, Rössler-type attractor; (b) $C_1 = 9.5$ nF, Double Scroll attractor; (c) $C_1 = 8.5$ nF, Double Scroll attractor.
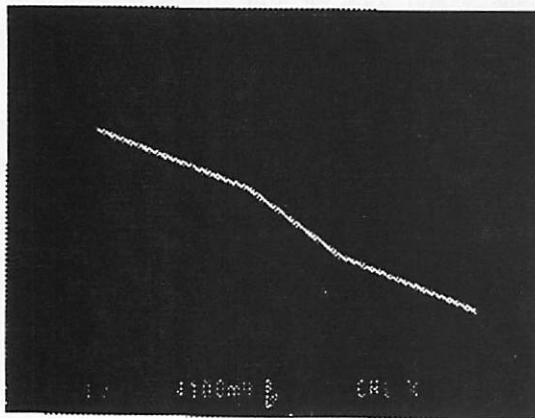
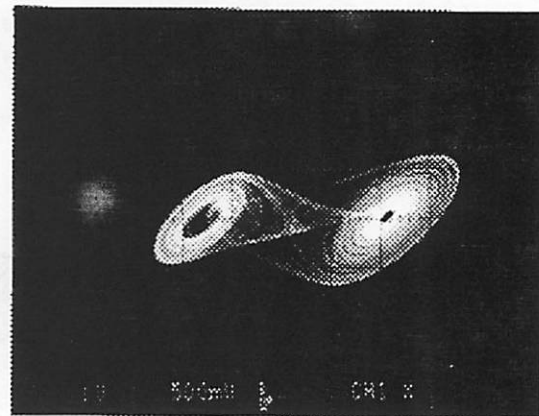(a)   (b)

Figure 18: When the attractor is too large, we cannot neglect the effects of the outer regions of the five-segment $v - i$ characteristic. (a) $C_1 = 10$nF: Double Scroll attractor is restricted to the regions of negative slope; (b) $C_1 = 8$nF: attractor is distorted by the outer positive-going segments.

(a)   (b)

Figure 19: Asymmetry induced by unequal positive and negative op amp saturation levels. (a) left breakpoint of the $v - i$ characteristic is smaller (in magnitude); (b) attractor is asymmetric.

20

If one wishes, the asymmetry due to saturation level mismatch may be corrected by adjusting the positive and negative power supply voltages until symmetry is achieved. For example, the negative saturation level might be 0.7V less in magnitude than the positive level. This could be corrected by using power supplies of 9V and -9.7V instead of ± 9V.

Normally, it is not possible to zero the offset in an eight-pin dual op amp such as the AD712 or the TL082. In fact, we deliberately chose the AD712 because it is draws negligible input current, by virtue to its FET input stage, and has a guaranteed maximum input offset voltage of 1.0mV (AD712K). If the offset is disturbing, one may substitute for the dual op amp two single op amp equivalents such as the AD711 and TL081; these have offset balancing pins to enable the user to set v_{OS} precisely equal to zero.

A superior realization of the Chua diode (in the sense that the breakpoints are independent of the saturation levels of the op amp and the slopes and breakpoints can be set independently) is described in [Ken92].

Finally, we note that the negative resistance converter in Fig. 7(a) exhibits a resistance of $-R_3$ over the central portion of its driving-point characteristic only when $R_2 = R_1$. Therefore, one should try to match the resistor pairs (R_1, R_2) and (R_4, R_5) in Fig. 10 as closely as possible.

9 Concluding remarks

Because Chua's circuit can exhibit a wide variety of nonlinear behaviors, it presents an attractive paradigm for experimental investigation of dynamical system. In this chapter, we have described a robust implementation of Chua's circuit. We have reviewed the circuit theoretic concepts underlying the design of negative resistors and have described a design strategy for synthesizing a five-segment piecewise-linear Chua diode by connecting two op amp negative resistance converters in parallel. Our example yields standard values allowing a working circuit to be assembled from off-the-shelf electronic components. We strongly encourage the reader to build this circuit and to explore the exciting world of nonlinear dynamics.

Acknowledgements

Appendix A VCVS-based negative resistance converter

Kirchhoff's current law (KCL) at node 1 in Fig. 5(a) gives:

$$i = \frac{1}{R_1}(v - v_o) \qquad (3)$$

Kirchhoff's voltage law (KVL) around loop 1-3-0-1 yields:

$$v = v_d + \frac{R_3}{R_2 + R_3}v_o \qquad (4)$$

The transfer function of the VCVS is given by

$$v_o = Av_d \qquad (5)$$

Hence, from equations (4) and (5),

$$v = \frac{R_2 + (1 + A)R_3}{A(R_2 + R_3)}v_o$$

Equivalently,

$$v_o = \frac{A(R_2 + R_3)}{R_2 + (1 + A)R_3}v$$

Substituting for v_0 in equation (3) gives

$$i = \frac{(1 - A)R_2 + R_3}{R_1[R_2 + (1 + A)R_3]}v$$

For large A,

$$i \approx -\frac{R_2}{R_1 R_3}v$$

Further, choosing $R_1 = R_2$ gives

$$i \approx -\frac{1}{R_3}v$$

This result is summarized graphically in Fig. 5(b).

Appendix B   Op amp-based negative resistance converter

The op amp is modeled as a VCVS with a three-segment piecewise-linear voltage transfer characteristic, as shown in Fig. 6(b). This model accounts for the nonzero DC offset v_{OS}, finite gain A in the linear region, and (possibly different) saturation levels $-E_{sat}^-$ and E_{sat}^+.

Negative saturation	$v_o = -E_{sat}^-$	$v_d \leq -\frac{E_{sat}^-}{A} + v_{OS}$
Linear	$v_o = A(v_d - v_{OS})$	$-\frac{E_{sat}^-}{A} + v_{OS} \leq v_d \leq \frac{E_{sat}^+}{A} + v_{OS}$
Positive saturation	$v_o = E_{sat}^+$	$v_d \geq \frac{E_{sat}^+}{A} + v_{OS}$

Table 2: Finite-gain op amp model with offset v_{OS}.

KCL at the non-inverting terminal of the op amp (node 1) in Fig. 7(a):

$$i = \frac{1}{R_1}(v - v_o) \tag{6}$$

KVL around loop 1-3-0-1:

$$v = v_d + \frac{R_3}{R_2 + R_3}v_o \tag{7}$$

We consider the three linear regions of the transfer characteristic separately.

Op amp in positive saturation

$$v_o = E_{sat}^+$$

Then, substituting for v_o in equation (6) gives

$$i = \frac{1}{R_1}v - \frac{1}{R_1}E_{sat}^+$$

The op amp is in positive saturation for

$$v_d \geq \frac{E_{sat}^+}{A} + v_{OS}$$

This is called the *validating equation* for the positive saturation region. Now

$$v = v_d + \frac{R_3}{R_2 + R_3}v_o$$

Thus, the validating equation becomes:

$$v \geq \frac{E_{sat}^+}{A} + v_{OS} + \frac{R_3}{R_2 + R_3}E_{sat}^+$$

$$v \geq \frac{R_2 + (1 + A)R_3}{A(R_2 + R_3)}E_{sat}^+ + v_{OS}$$

This corresponds to the rightmost segment of the $v - i$ characteristic in Fig. 7(b). The breakpoint is defined by

$$B_P^+ = \frac{R_2 + (1 + A)R_3}{A(R_2 + R_3)}E_{sat}^+ + v_{OS}$$

23

and the slope by

$$m_0 = \frac{1}{R_1}$$

For large A,

$$B_P^+ \approx \frac{R_3}{R_2 + R_3} E_{sat}^+ + v_{OS}$$

Op amp in negative saturation

Substituting $v_o = -E_{sat}^-$ for $v_o = E_{sat}^+$ in the above analysis yields the leftmost segment of the $v - i$ characteristic in Fig. 7(b). $m_0 = 1/R_1$ as before, and the validating equation gives

$$-B_P^- = -\frac{R_2 + (1 + A)R_3}{A(R_2 + R_3)} E_{sat}^- + v_{OS}$$

as the upper bound of the negative saturation region.

Op amp in linear region

In the linear region,

$$v_o = A(v_d - v_{OS})$$

Substituting for v_o in equation (6) gives

$$i = \frac{1}{R_1}v - \frac{1}{R_1}A(v_d - v_{OS}) \tag{8}$$

Now, from equation (7),

$$
\begin{aligned}
v &= v_d + \frac{R_3}{R_2 + R_3} v_o \\
&= v_d + \frac{R_3}{R_2 + R_3} A(v_d - v_{OS}) \\
&= \frac{R_2 + (1 + A)R_3}{R_2 + R_3} v_d - \frac{AR_3}{R_2 + R_3} v_{OS}
\end{aligned}
$$

Rewriting v_d in terms of v gives:

$$v_d = \frac{R_2 + R_3}{R_2 + (1 + A)R_3} v + \frac{AR_3}{R_2 + (1 + A)R_3} v_{OS} \tag{9}$$

and

$$v_d - v_{OS} = \frac{R_2 + R_3}{R_2 + (1 + A)R_3}(v - v_{OS})$$

Substituting for $(v_d - v_{OS})$ in terms of v in equation (8) gives:

$$i = \frac{(1 - A)R_2 + R_3}{R_1[R_2 + (1 + A)R_3]} v + \frac{A(R_2 + R_3)}{R_1[R_2 + (1 + A)R_3]} v_{OS}$$

For large A,

$$i \approx -\frac{R_2}{R_1 R_3} v + \frac{R_2 + R_3}{R_1 R_3} v_{OS}$$

The op amp is in its linear region when

$$-\frac{E_{sat}^-}{A} + v_{OS} \leq v_d \leq \frac{E_{sat}^+}{A} + v_{OS}$$

Equivalently, substituting for v_d from equation (9),

$$-\frac{E_{sat}^-}{A} + v_{OS} \leq v_d = \frac{R_2 + R_3}{R_2 + (1 + A)R_3}v + \frac{AR_3}{R_2 + (1 + A)R_3}v_{OS} \leq \frac{E_{sat}^+}{A} + v_{OS}$$

Hence, the op amp is in its linear region for

$$-\frac{R_2 + (1 + A)R_3}{A(R_2 + R_3)}E_{sat}^- + v_{OS} \leq v \leq \frac{R_2 + (1 + A)R_3}{A(R_2 + R_3)}E_{sat}^+ + v_{OS}$$

For large A, this reduces to

$$-\frac{R_3}{R_2 + R_3}E_{sat}^- + v_{OS} \leq v \leq \frac{R_3}{R_2 + R_3}E_{sat}^+ + v_{OS}$$

Consider once again Fig. 7(b). We have that

$$m_1 = \frac{(1 - A)R_2 + R_3}{R_1[R_2 + (1 + A)R_3]}$$

and

$$OS = -\frac{A(R_2 + R_3)}{(1 - A)R_2 + R_3}v_{OS}$$

For large A,

$$m_1 \approx -\frac{R_2}{R_1 R_3}$$

and

$$OS \approx -\frac{R_2 + R_3}{R_2}v_{OS}$$

Appendix C Parallel connection of two negative resistance converters

We connect in parallel two negative resistance converters N_{R2} and N_{R1} as shown in Fig. 8. Nonlinear resistor N_{R_1} has a three-segment piecewise-linear characteristic with slopes m_{01} and m_{11} and breakpoints $\pm B_{P1}$ (as in Fig. 9(b)). Similarly, N_{R_2} has slopes m_{02} and m_{12} and breakpoints $\pm B_{P2}$ (Fig. 9(a)). The compound five-segment characteristic has slopes m_{-1}, m_0, and m_1 and two pairs of breakpoints at $\pm B_{P1}$ and $\pm B_{P2}$ (as in Fig. 9(c)).

From the continuity of the $v - i$ characteristic of N_{R2}, we have

$$- B_{P2}m_{12} = (E_{sat} - B_{P2})m_{02} \tag{10}$$

Thus

$$E_{sat}m_{02} = B_{P2}(m_{12} - m_{02})$$

But, from equation (3),

$$m_{02} - m_{12} = m_0 - m_1$$

giving

$$m_{02} = \frac{B_{P2}}{E_{sat}}(m_0 - m_1)$$

From equation (10),

$$
\begin{aligned}
m_{12} &= \frac{B_{P2} - E_{sat}}{B_{P2}}m_{02} \\
&= \frac{B_{P2} - E_{sat}}{E_{sat}}(m_0 - m_1)
\end{aligned}
$$

From equation (3),

$$
\begin{aligned}
m_{11} &= m_1 - m_{12} \\
&= \frac{B_{P2}m_1 + (E_{sat} - B_{P2})m_0}{E_{sat}}
\end{aligned}
$$

From the continuity of the $v - i$ characteristic of N_{R1},

$$-B_{P1}m_{11} = (E_{sat} - B_{P1})m_{01}$$

Thus

$$m_{01} = \frac{B_{P1}}{B_{P1} - E_{sat}}m_1$$

References

[Ana90]   Analog Devices, Inc. *Linear Products Databook 1990/91*, 1990.

[Ana91]   Analog Devices, Inc. SPICE model library, 1991. Release C 1/91.

[BC88]   P. Bartissol and L. O. Chua. The Double Hook. *IEEE Trans. Circuits Syst.*, CAS-35(12):1512—1522, 1988.

[Bro87]   M. E. Broucke. One-parameter bifurcation diagram for Chua's circuit. *IEEE Trans. Circuits Syst.*, CAS-34(3):208—209, 1987.

[BT90]   C. M. Blazquez and E. Tuma. Dynamics of the Double Scroll circuit. *IEEE Trans. Circuits Syst.*, CAS-37(5):589—593, 1990.

[CC91]   J. Cruz and L. O. Chua. First ic implementation of nonlinear resistor in Chua's circuit. (preliminary report), 1991.

[CDK87]   L. O. Chua, C. A. Desoer, and E.S. Kuh. *Linear and Nonlinear Circuits*. McGraw-Hill, New York, 1987.

[CKM86]   L. O. Chua, M. Komuro, and T. Matsumoto. The Double Scroll family, parts I and II. *IEEE Trans. Circuits Syst.*, CAS-33(11):1073—1118, 1986.

[CL90a]   L. O. Chua and G. N. Lin. Canonical realization of Chua's circuit family. *IEEE Trans. Circuits Syst.*, CAS-37(7):885—902, 1990.

[CL90b]   L. O. Chua and G. N. Lin. Intermittency in a piecewise-linear circuit. *IEEE Trans. Circuits Syst.*, CAS-38(5):510—520, 1990.

[JQN+91]   B. Johnson, T. Quarles, A. R. Newton, D. O. Pederson, and A. Sangiovanni-Vincentelli. SPICE3 version 3e user's manual. ERL memorandum, Electronics Research Laboratory, University of California at Berkeley, CA 94720, 1991.

[Kah88a]   C. Kahlert. The chaos producing mechanism in Chua's circuit. *Int. J. Circuit Theory Appl.*, 16(4):227—232, 1988.

[Kah88b]   C. Kahlert. Dynamics of the inclusions appearing in the return maps of Chua's circuit - 1. the creation mechanism. *Int. J. Circuit Theory Appl.*, 17(1):29—46, 1988.

[Kah88c]   C. Kahlert. The range of transfer and return maps in three-region piecewise-linear dynamical systems. *Int. J. Circuit Theory Appl.*, 16:11—23, 1988.

[Kah91]   C. Kahlert. Heteroclinic orbits and scaled similar structures in the parameter space of the Chua oscillator. In G. Baier and M. Klein, editors, *Chaotic Hierarchy*, pages 209—234. World Scientific, Singapore, 1991.

[KC87]   C. Kahlert and L. O. Chua. Transfer maps and return maps for piecewise-linear and three-region dynamical systems. *Int. J. Circuit Theory Appl.*, 15:23—49, 1987.

[KC91]   M. P. Kennedy and L. O. Chua. Hysteresis in electronic circuits: A circuit theorist's perspective. *Int. J. Circuit Theory Appl.*, 19(5):471–515, 1991.

[Ken92]   M. P. Kennedy. Design notes for Chua's circuit. ERL memorandum, Electronics Research Laboratory, University of California at Berkeley, CA 94720, 1992.

[Kom88a]   M. Komuro. Normal forms of continuous piecewise-linear vector fields and chaotic attractors: Part I. *Japan J. Appl. Math*, 5(2):257—304, 1988.

[Kom88b] M. Komuro. Normal forms of continuous piecewise-linear vector fields and chaotic attractors: Part II. *Japan J. Appl. Math*, 5(3):503—549, 1988.

[Kom90] M. Komuro. Bifurcation equations of 3-dimensional piecewise-linear vector fields. In H. Kawakami, editor, *Bifurcation Phenomena in Nonlinear Systems and Theory of Dynamical Systems*, pages 113—123. World Scientific, Singapore, 1990.

[KTMH91] M. Komuro, R. Tokunaga, T. Matsumoto, and A. Hotta. Global bifurcation analysis of the Double Scroll circuit. *Int. J. Bifurcation and Chaos*, 1(1):139—182, 1991.

[LU91] R. Lozi and S. Ushiki. Confinors and bounded-time patterns in Chua's circuit and the Double Scroll family. *Int. J. Bifurcation and Chaos*, 1(1):119—138, 1991.

[Mat84] T. Matsumoto. A chaotic attractor from Chua's circuit. *IEEE Trans. Circuits Syst.*, CAS-31(12):1055—1058, 1984.

[MC87] A. I. Mees and P. B. Chapman. Homoclinic and heteroclinic orbits in the Double Scroll attractor. *IEEE Trans. Circuits Syst.*, CAS-34(9):1115—1120, 1987.

[MCA88] T. Matsumoto, L. O. Chua, and K. Ayaki. Reality of chaos in the Double Scroll circuit: A computer-assisted proof. *IEEE Trans. Circuits Syst.*, CAS-35(7):909—925, 1988.

[MCK85] T. Matsumoto, L. O. Chua, and M. Komuro. The Double Scroll. *IEEE Trans. Circuits Syst.*, CAS-32(8):797—818, 1985.

[MCK86] T. Matsumoto, L. O. Chua, and M. Komuro. The Double Scroll bifurcations. *Int. J. Circuit Theory Appl.*, 14(1):117—146, 1986.

[MCK87] T. Matsumoto, L. O. Chua, and M. Komuro. Birth and death of the Double Scroll. *Physica*, 24D:97—124, 1987.

[MCT86] T. Matsumoto, L. O. Chua, and K. Tokumasu. Double Scroll via a two-transistor circuit. *IEEE Trans. Circuits Syst.*, CAS-33(8):828—835, 1986.

[MCT87] T. Matsumoto, L. O. Chua, and R. Tokunaga. Chaos via torus breakdown. *IEEE Trans. Circuits Syst.*, CAS-34(3):240—253, 1987.

[Ogo87] M. J. Ogorzalik. Chaotic regions from Double Scroll. *IEEE Trans. Circuits Syst.*, CAS-34(2):201—203, 1987.

[PC87a] T. S. Parker and L. O. Chua. The dual Double Scroll equation. *IEEE Trans. Circuits Syst.*, CAS-34(9):1059—1073, 1987.

[PC87b] T. S. Parker and L. O. Chua. INSITE — a software toolkit for the analysis of nonlinear dynamical systems. *Proc. IEEE*, 75(8):1081–1089, 1987.

[Ras90] M. H. Rashid. *SPICE for Circuits and Electronics using PSpice*. Prentice-Hall, Englewood Cliffs, N.J., 1990.

[SC88] C. P. Silva and L. O. Chua. The overdamped Double Scroll family. *Int. J. Circuit Theory Appl.*, 16(7):223—302, 1988.

[Tex90] Texas Instruments. *Operational Amplifier Macromodels — Linear Circuits Data Manual*, 1990.

[TMIM89] R. Tokunaga, T. Matsumoto, T. Ida, and K. Miya. Homoclinic linkage in the Double Scroll circuit and the cusp-constrained circuit. In N. Aoki, editor, *The Study of Dynamical Systems*, pages 192—209. World Scientific, Singapore, 1989.

[TMK+89] R. Tokunaga, T. Matsumoto, M. Komuro, L. O. Chua, and K. Miya. Homoclinic linkage: A new bifurcation mechanism. *Proc. IEEE ISCAS*, 2:826—829, 1989.

[Wu87]   S. Wu. Chua's circuit family. *Proc. IEEE*, 75(8):1022—1032, 1987.

[YL87]   L. Yang and Y. L. Liao. Self-similar structures from Chua's circuit. *Int. J. Circuit Theory Appl.*, 15:189—192, 1987.

[ZA85a]   G. Q. Zhong and F. Ayrom. Experimental confirmation of chaos from Chua's circuit. *Int. J. Circuit Theory Appl.*, 13(11):93—98, 1985.

[ZA85b]   G. Q. Zhong and F. Ayrom. Periodicity and chaos in Chua's circuit. *IEEE Trans. Circuits Syst.*, CAS-32(5):501—503, 1985.